Supplementary Information

Phosphoinositides regulate the TCR/CD3 complex membrane dynamics and activation

Nassima Chouaki Benmansour[1], Kilian Ruminski[1], Anne-Marie Sartre[1], Marie-Claire Phelipot[1], Audrey Salles[1,5], Elise Bergot[1], Ambroise Wu[1], Gaëtan Chicanne[2], Mathieu Fallet[1] Sophie Brustlein[1], Cyrille Billaudeau[1,6], Anthony Formisano[1], Sébastien Mailfert[1], Bernard Payrastre[2,3], Didier Marguet[1], Sophie Brasselet[4], Yannick Hamon[1] & Hai-Tao He[1]

[1] Aix Marseille Univ, CNRS, INSERM, CIML, Centre d'Immunologie de Marseille-Luminy, Marseille, France

[2] Institut des Maladies Métaboliques et Cardiovasculaires, Inserm U1048, Université Toulouse 3, Toulouse, France

[3] Laboratoire d'Hématologie, Centre Hospitalier Universitaire de Toulouse, Toulouse, France

[4] Aix-Marseille Univ, CNRS, Centrale Marseille, Institut Fresnel, UMR 7249, 13397 Marseille, France

[5] Current address: UTechS Photonic BioImaging (Imagopole) Citech, Institut Pasteur, Paris, 75015, France

[6] Current address: Micalis Institute, INRA, AgroParisTech, Université Paris-Saclay, 78350 Jouy-en-Josas, France

Yannick Hamon & Hai-Tao He contributed equally to this work. Correspondence and requests for materials should be addressed to Y.H. (hamon@ciml.univ-mrs.fr) or H.-T.H. (he@ciml.univ-mrs.fr)

The Supplementary Information includes six supplementary figures (Figures S1 – S6) and one supplementary table (Table S1).

Figure S1

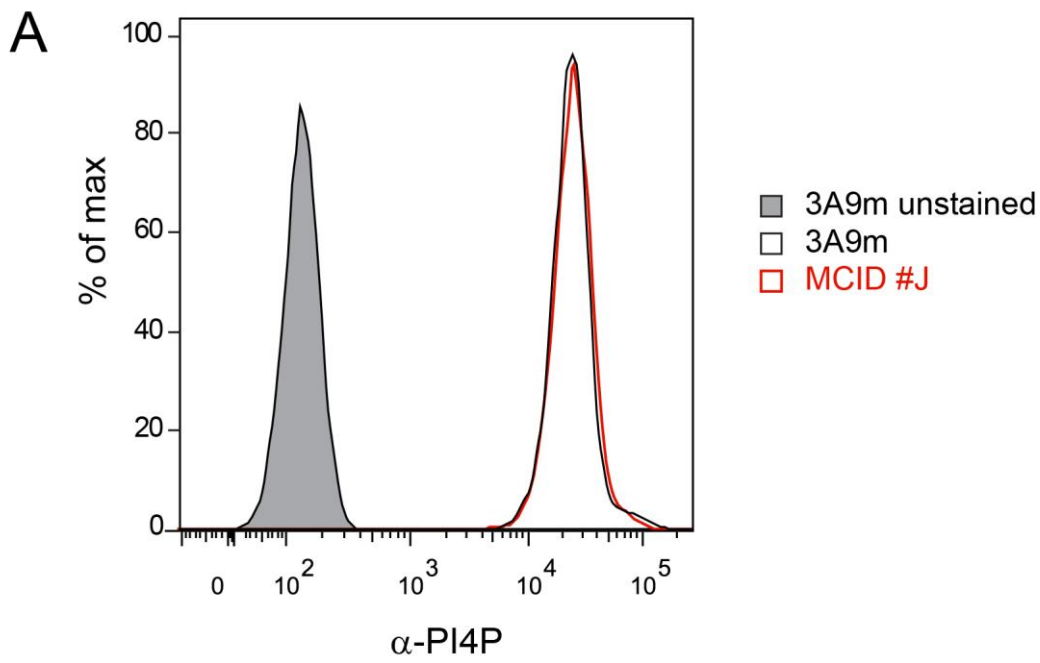
A
100
80
60
40
20
0
% of max
0
10^2
10^3
10^4
10^5
α-PI4P
3A9m unstained
3A9m
MCID #J

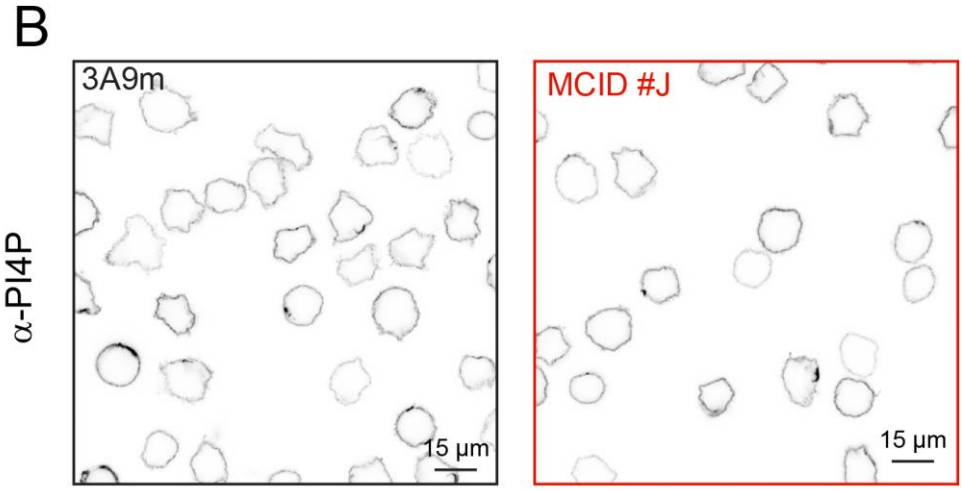
B
α-PI4P
3A9m
15 µm
MCID #J
15 µm

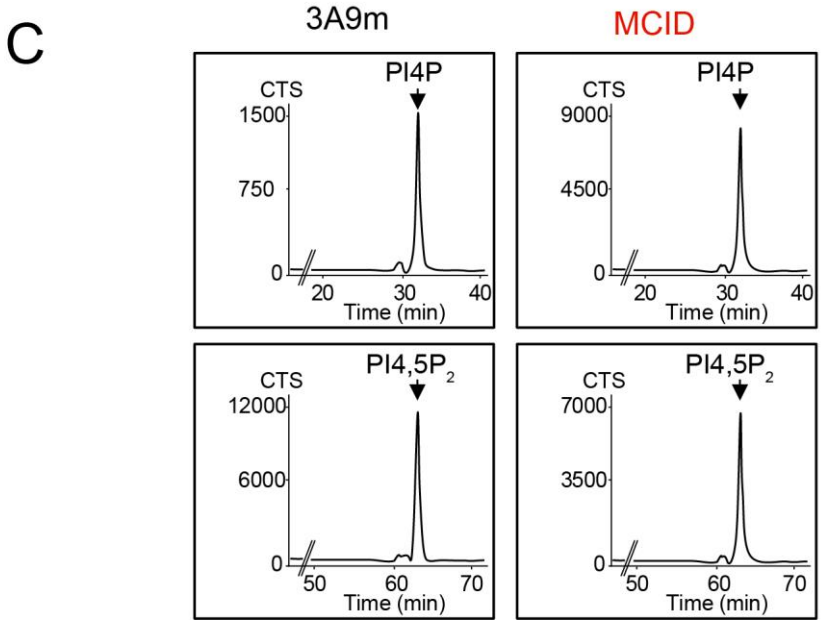
C
3A9m
MCID
PI4P
CTS
1500
750
0
9000
4500
20
30
40
Time (min)
PI4,5P2
12000
6000
7000
3500
50
60
70

Figure S1: Analysis of PI4P levels upon MCID expression

(A) Flow cytometry analysis of the PI4P PM level in 3A9m and MCID #J cells, espectively. The unstained control is shown in gray.

(B) Confocal images of the anti-PI4P mAb labelled cells in (A).

(C) HPLC profile of PI4P and PI(4,5)P_2 extracted from [^{32}Pi]-orthophosphate labelled 3A9m WT and MCID cells, respectively (see Methods for details).

Figure S2

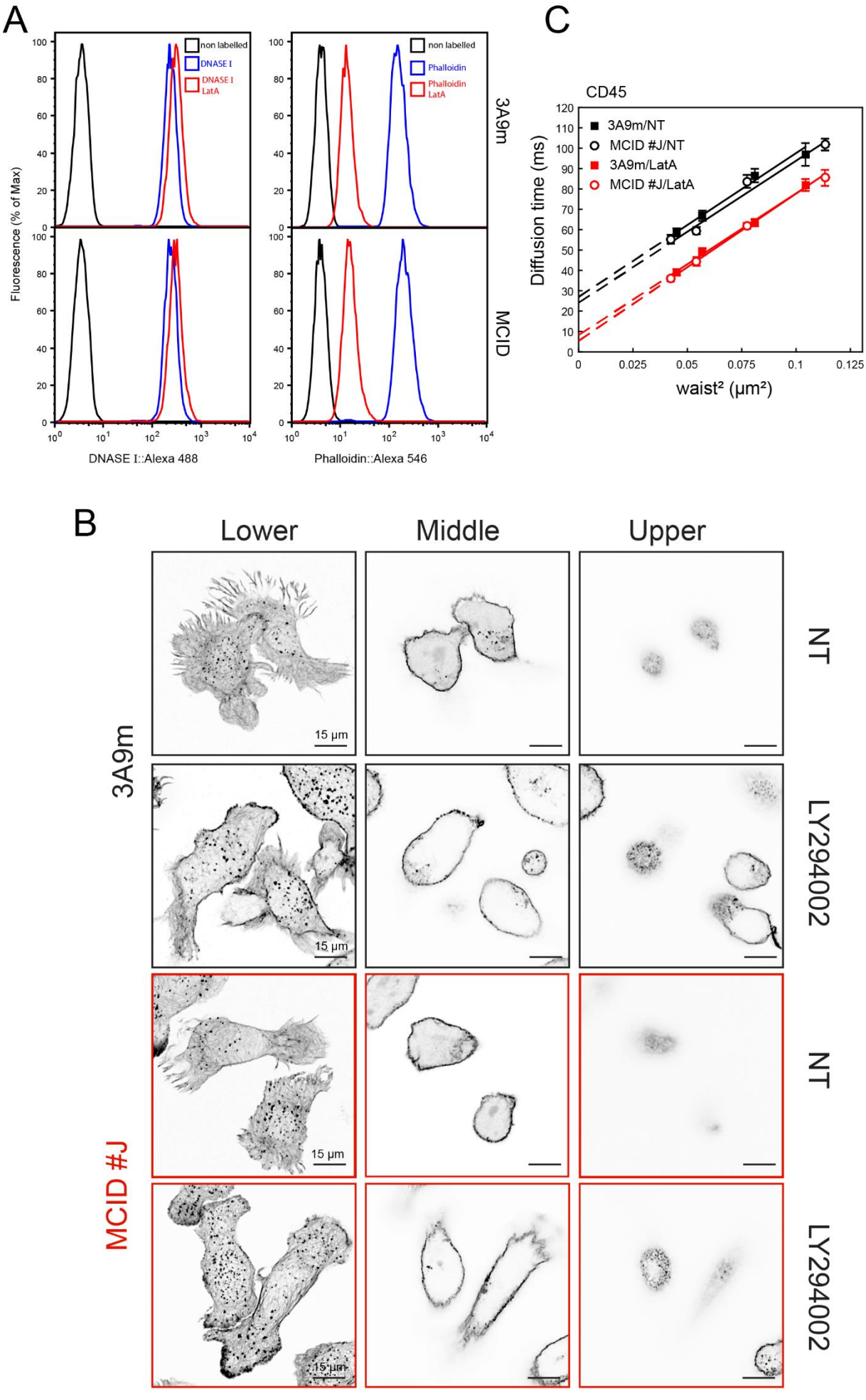
A
non labelled
DNASE I
DNASE I LatA
Phalloidin
Phalloidin LatA
3A9m
MCID
Fluorescence (% of Max)
DNASE I::Alexa 488
Phalloidin::Alexa 546
C
CD45
3A9m/NT
MCID #J/NT
3A9m/LatA
MCID #J/LatA
Diffusion time (ms)
waist² (µm²)
B
Lower
Middle
Upper
3A9m
MCID #J
NT
LY294002
NT
LY294002
15 µm

Figure S2: The MCID expression minimally affects the organization of the F-actin cortex

(A) Flow cytometry analysis with Alexa 488-conjugated DNASE 1 (left panels) and Alexa 546-conjugated phalloidin (right panels) of the untreated (in blue) or Latruncunlin A (that induces actin depolymerization, 2.5µM) treated (in red) 3A9m WT or MCID cells, respectively.

(B) Super-resolution microscopy of the actin cytoskeleton architecture of the antibody-immobilized 3A9m or MCID #J cells, treated or not with PI3K inhibitor LY294002 before being stained with Alexa 647-conjugated phalloidin and imaged by the confocal microscopy enhanced with airyscan technology. Lower, middle and upper optical sections are shown from a Z-stack acquisition (see Methods for details). These data, together with those shown in (A), depicted an overall preserved actin cortex architecture upon MCID expression. In addition, no difference in the actin cortex organization could be found between 3A9m and MCID #J cells after inhibition of the PI3K activity to deplete PI(3,4,5)P3.

(C) svFCS analysis of the PM lateral diffusion of CD45 labelled with Alexa 488::H193.16.3 Fab, in non-treated (in black) and Latruncunlin A-treated (in red) 3A9m or MCID #J cells, respectively. The lateral diffusion of CD45 in the PM of T cells is known to be constrained by the cortical actin cytoskeleton[1]. The highly sensitive svFCS technique[2,3] in combination with Latruncunlin A treament allowed establishing that the F-actin-constrained lateral diffusion for CD45 was unchanged upon MCID expression, indicating a normal cortical actin cytoskeleton in the MCID-expressing cells (see Methods for the details of svFCS analysis).

Figure S3

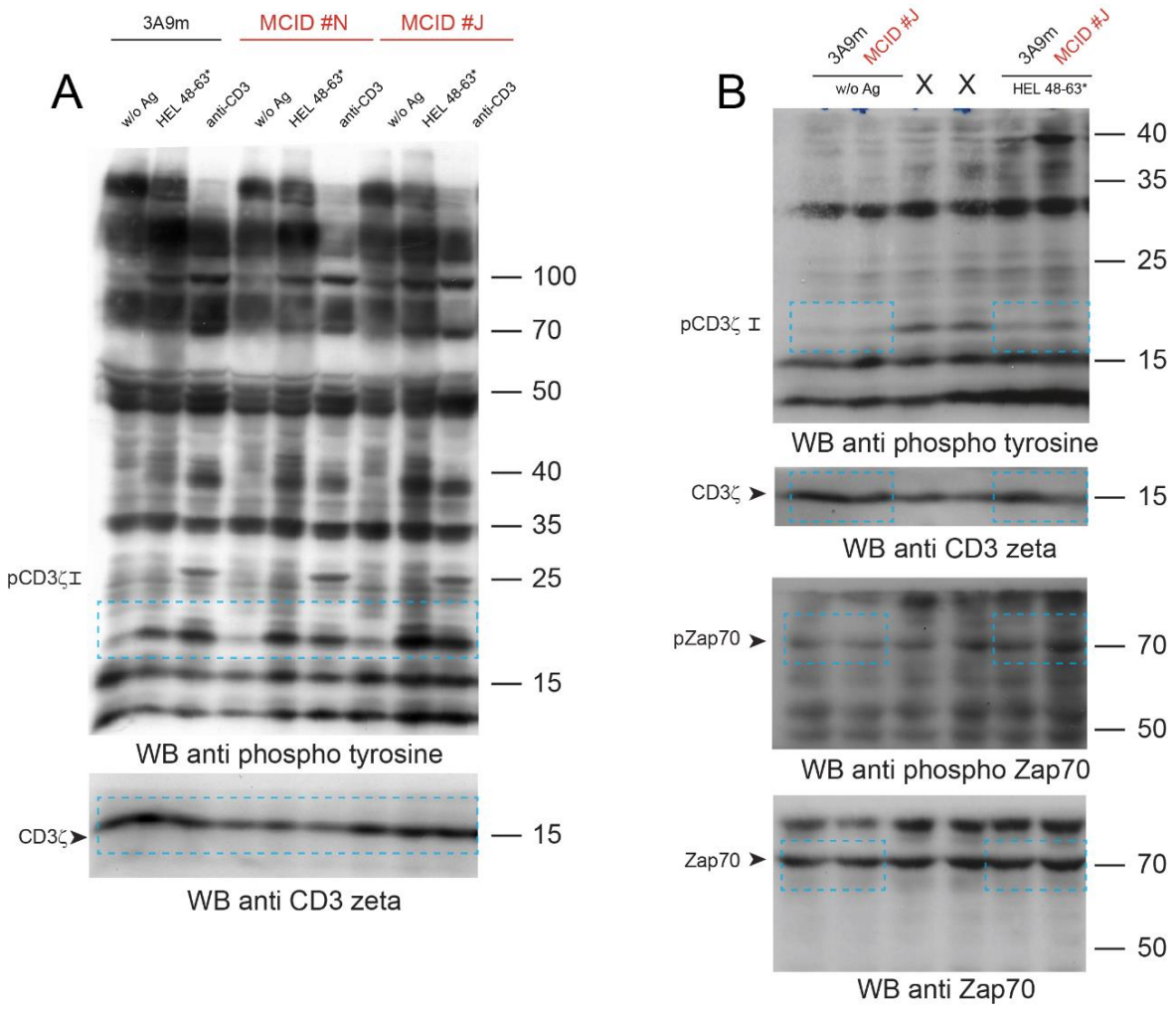

Figure S3: Uncropped images of immunoblots shown in Figure 2

(A) 3A9m mock-transfected WT cells or MCID #N or #J clones were seeded onto COS-A^k or COS-$A^k_{48\text{-}63}$* cells, or incubated with soluble anti-CD3ε mAb (145-2C11, 10 µg/ml), for 5 min at 37°C. Cell lysates were immunoblotted with an anti-p-Tyr mAb (4G10) to detect the phosphorylated isoforms of CD3ζ (p21 and p23). The bottom portion of the blot was stripped and reprobed with an anti-CD3ζ antibody to detect the (p16) CD3ζ molecule.

(B) The experiment was carried out same as that in (A), except that only the lower portion of the blot was analyzed with anti-p-Tyr mAb to detect the phosphorylated isoforms of CD3ζ (p21 and p23), while the upper portion of the blot was analyzed with an anti-p-Zap-70 antibody to detecet phosphorylation of Zap-70 (pTyr 319). The bottom portion of the blot was stripped and

reprobed with an anti-CD3ζ antibody to detect the (p16) CD3ζ molecule. The upper portion of the blot was stripped and reprobed with an anti-Zap-70 mAb to detect the Zap-70 molecule.

Figure S4

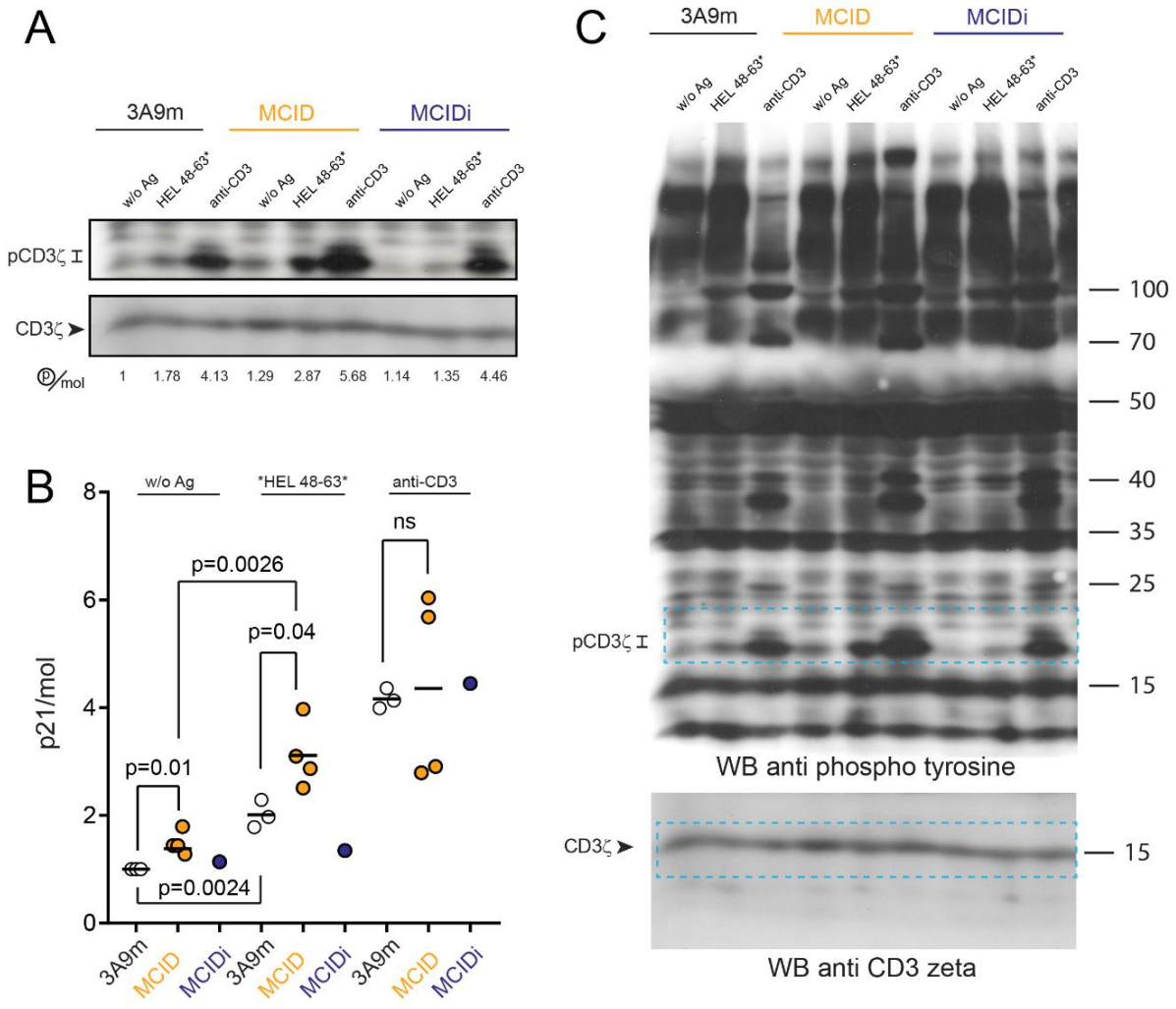

Figure S4: The increased TCR activation upon MCID expression

(A) 3A9m WT, MCID or MCIDi cells were seeded onto COS-A^k or COS-$A^k_{48\text{-}63}$* cells, or incubated with anti-CD3ε mAb (145-2C11, 10 µg/ml) for 5 min at 37°C. Cell lysates were immunoblotted with an anti-p-Tyr mAb (4G10) to detect the phosphorylated isoforms of CD3ζ (p21 and p23). The bottom portion of the blot was stripped and reprobed with an anti-CD3ζ antibody to detect the (p16) CD3ζ molecule.

(B) Statistical analysis of the p21/CD3ζ ratio from 3 independent immunoblots performed as in (A) for 3A9m, MCID and MCIDi quantification in (A) is plotted as a control.

(C) Uncropped version of the immunoblots shown in (A).

Figure S5

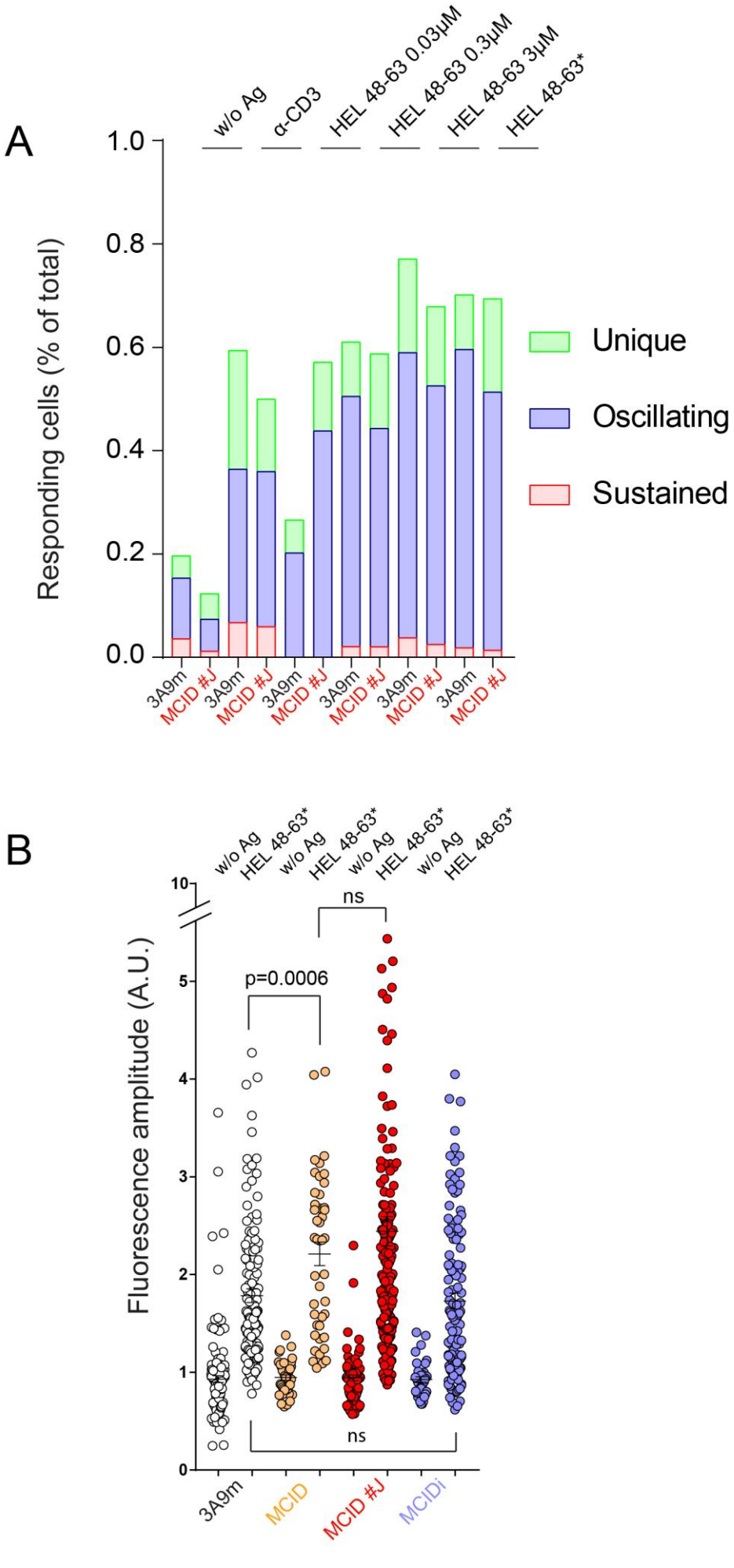
A
w/o Ag
α-CD3
HEL 48-63 0.03μM
HEL 48-63 0.3μM
HEL 48-63 3μM
HEL 48-63*
Responding cells (% of total)
1.0
0.8
0.6
0.4
0.2
0.0
Unique
Oscillating
Sustained
3A9m
MCID #J
B
w/o Ag
HEL 48-63*
Fluorescence amplitude (A.U.)
10
5
4
3
2
1
0
p=0.0006
ns
ns
3A9m
MCID
MCID #J
MCIDi

Figure S5: The increased TCR-mediated Ca^{2+} store release upon MCD expression

(A) Percentage of cells over the activation threshold in the calcium imaging experiment of Fig. 2d.

(B) Comparative analysis of the fluorescence amplitude of individual cells over the threshold in 3A9m WT, 3A9m MCID, MCID #J and MCIDi cells upon incubation with COS-A^k cells or COS-$A^k_{48\text{-}63}$*.

Figure S6

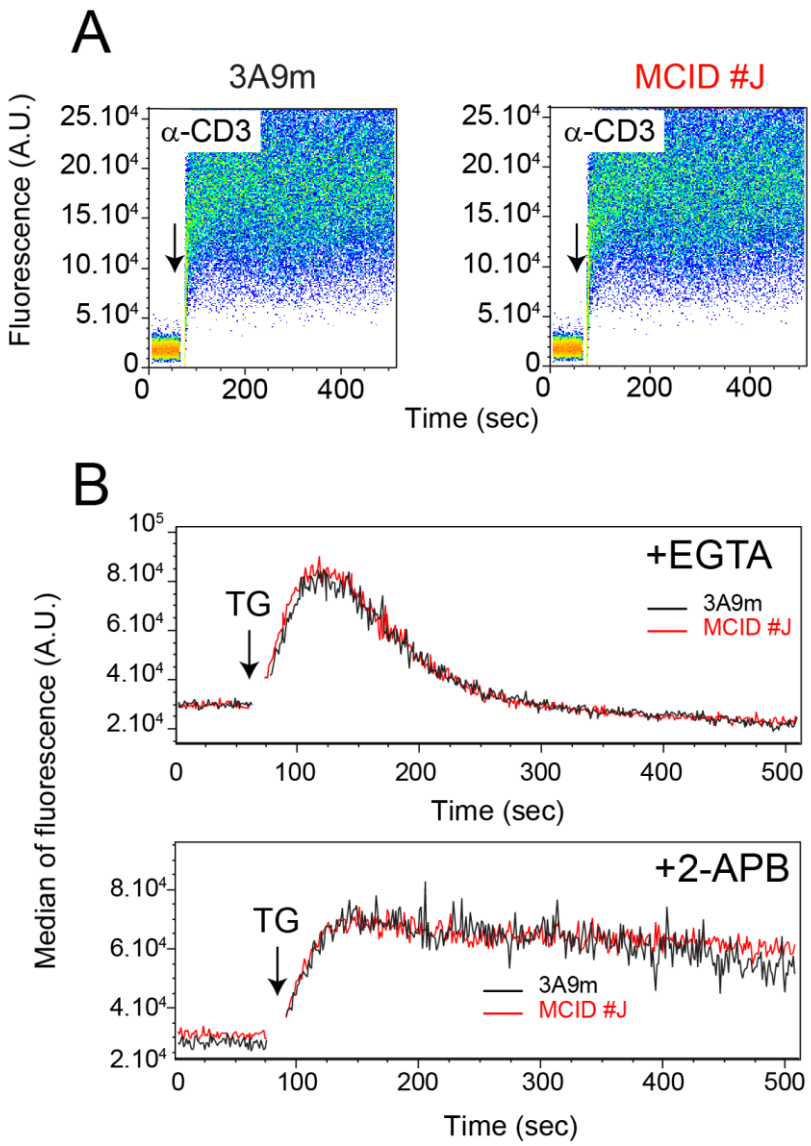

Figure S6: Flow cytometry analysis of soluble anti-CD3 mAb binding and the Ca^{2+} store release stimulted by thapsigargin

(A) Alexa 488-conjugated anti-CD3ε mAb binding kinetics on 3A9m (left panel) or MCID #J (right panel) cells were analyzed by flow cytometry and plotted over time as indicated in Methods. Autofluorescence was recorded for 1 min (and considered as the baseline) prior to addition of soluble fluorescent anti-CD3ε mAb (5 µg/ml).

(B) Calcium mobilization response upon stimulation with thapsigargin. Cells were stimulated upon addition of 0.1 µM thapsigargin (arrow) in the presence of 1 mM EGTA (upper panel) or 10 µM 2-APB (lower panel). Median of fluorescence are expressed as a function of time.

Construct		Oligos sequences	Strategy	Cloned into	Sites	Amplification matrix
Lck1-12::mCherry::INP54d (MCID)	For	GTCGTAACAACTCCGC	PCR overlap extension	pEGFPm-N2	EcoRI/NotI	pEGFP-N2m Lck1-12 (Cf Lasserre, R. Nat Chem Biol, 20
	Rev	CCCGCGCCGGCTCCTGCGGATCCCCTTGTACAGCTCGTCCAT				
	For	GGGATCCGCAGGAGCCGGCGCGGGATGAACAAAACGAATTGGA				pCDNA3 lyn::EGFP::INP54 (gift from Jaques Nunes)
	Rev	AAAGGAAAAAGCGGCCGCTTACGGCACTGGCGTCC				
Lck1-12::mCherry::INP54d D311G	For	CAATGCTCTATTATTTAGCGGTCATCAACCCGTTAATC	Quikchange mutagenesis	NA	NA	MCID
	Rev	GATTAACGGGTTGATGACCGCTAAATAATAGAGCATTG				
Lck1-12::mCherry::INP54d D311G D280A (MCI	For	CCGTCGTGGTGCGCTAGGATTCTCTACAAAAGC	Quikchange mutagenesis	NA	NA	Lck1-12::mCherry::INP54 D311G
	Rev	GCTTTTGTAGAGAATCCTAGCGCACCACGACGG				
CD3e::EGFPm	For	AAGAGCTTCGAATTCACCATGCGGTGGAACACTTTC	PCR *in* -fusion cloning	pEGFPm-N2	EcoRI/BamHI	mouse CD3 epsilon cDNA (gift from Bent Rubin)
	Rev	ACCGGCCGTGGATCCCGACTGCACTCTGATTCAG				
CD3e::EGFPm R183S	Rev	ACCGGCCGTGGATCCCGACTGCACTCTGATTCAG	PCR *in* -fusion cloning	pEGFPm-N2	EcoRI/BamHI	idem
CD3e::EGFPm Δ N181+	Rev	ACCGGCCGTGGATCCCAGGCCAGAATACAGGT	PCR *in* -fusion cloning	pEGFPm-N2	EcoRI/BamHI	idem
CD3e::EGFPm Δ K171+	Rev	ACCGGCCGGACGTGGATCCCGCGGATGGGCTCATAG	PCR *in* -fusion cloning	pEGFPm-N2	EcoRI/BamHI	idem
CD3e::EGFPm Δ N163+	Rev	ACCGGCCGGTGGATCCCGGCAACAGGTGGTGGC	PCR *in* -fusion cloning	pEGFPm-N2	EcoRI/BamHI	idem
CD3e::EGFPm Δ P158+	Rev	ACCGGCCGGTGGATCCCCGCTCCTTGTTTGCC	PCR *in* -fusion cloning	pEGFPm-N2	EcoRI/BamHI	idem
CD3e FF::EGFPm	For	CCCAACCCAGACTTTGACCCCATCCGCAAAGGCCAGCGGGACCTGTTTTCTGGCCTG	Quikchange mutagenesis	NA	NA	idem
	Rev	CAGGCCAGAAAACAGGTCCCGCTGGCCTTTGCGGATGGGCTCAAAGTCTGGGTTGGG				
CD3eCD:: EGFPm	For	ACGCGTCGACCGCCACCATGGTGAGCAAGAATAGGAAGGC	PCR cloning	pEGFPm-N2	SalI/BamHI	idem
	Rev	CGCTGGATCCCGACTGCACTCTGATTCAG				
myr::EGFPm	For	AATTCCGCCACCATGGGCAGTGTCAGCAGCTCAAACCCTGAAGATGAC	Annealed oligos	pEGFPm-N2	EcoRI/SalI	NA
	Rev	GATTCATCTTCAGGGTTTGAGCTGCTGACACTGCCCATGGTGGCGG				
myr::CD3eCD::EGFPm (Lck1-12_3_Pstn_P.le_P.le reversed reverse)	For	CGGGAATTCCGCCACCATGGGCAGTGTCAGCAGCTCAAACCCTGAAGATGACTGGAGCAAGAATAGGAAG	PCR cloning	pEGFPm-N2	EcoRI/SalI	mouse CD3 epsilon cDNA (gift from Bent Rubin)
	Rev	ACGGTCGACTGCCCCCTCCACCGACTGCACTCTGATTCAG				
Lck 1-12::CD3eCD::EGFPm	For	TACCATATGGGCTGTGTCTGCAGCTCAAACCCT	Quikchange mutagenesis	NA	NA	myr::CD3eCD::mEGFP
	Rev	AGGGTTTGAGCTGCAGACACAGCCCATGGTA				
Lck1-1-12::CD3eCD_KS::EGFPm	For	GAAGATGACTGGAGCAGCAATAGTAGCGCCTCGGCCAGCCCTGTGACCTCAGGTACCGGTGCTGGTAGCAGGCCC	Quikchange mutagenesis	NA	NA	Lck1-1-12::CD3eCD::EGFPm
	Rev	GGGCCTGCTACCAGCACCGGTACCTGAGGTCACAGGGCTGGCCGAGGCGCTACTATTGCTGCTCCAGTCATCTTC				
Lck::EGFP	For	TAATACGACTCACTATAGG	PCR overlap extension	pDNA 3.1(+)	Hind III/NotI	pCDNA 3 Lck
	Rev	GCTTCCACCGCCTCCAGGCTGGGCTGGTA				
	For	GGAGGCGGTGGAAGCATGGTGAGCAAGGGCG				pEGFP-N2m Lck1-12 (Cf Lasserre, R. Nat Chem Biol, 20
	Rev	AAGAATGCGGCCGCTTTACTTGTACAGCTCGTC				
Lactadherin GFP	For	GCAGACAGATCTTGCACTGAACCCTAG	PCR	pEGFPm-C1	BglII/EcoRI	Bovine Lactadherin cDNA
	Rev	GCAGACGAATTCCTAACAGCCCAGCAG				
(PH PLCδ)²	For	CCGGAATTCTATGGACTCGGCCGG	PCR	pEGFPm-C2 PH_PLCδ	EcoRI/BamHI	PH PLCδ cDNA (Gift from Georges Bismuth)
	Rev	CGCGGATCCTCTGCCCCTCCACCCTGGATGTTGAGCTCCT				
Lck1-12::EGFPm::Hras Cterm	For	GTACAAGCCCGGGTGCATGAGCTGCAAGTGTGTCTCCTAAAGC	Annealed oligos	pEGFPm-N2 Lck1-12	BsrGI/NotI	NA
	Rev	GGCCGCTTTAGGAGCACACATCTTGCAGCTCATGCACCCGGGCTT				
Lck1-12::EGFPm::MARCKS ED	For	GTACAAGTTCGGACTCGCTTCTAAGAATAGGAAGGCCAAGGCCAAGCCTGTGACCCGAGGAACCGGTGCTGGTAGCAGGCCCAGAGGGCAACAACAAGGAGCGGTAAGC	Annealed oligos	pEGFPm-N2 Lck1-12	BsrGI/NotI	NA
	Rev	GGCCGCTTACCGCTCCTTGTTTTGCCCTCTGGGCCTGCTACCAGCACCGGTTCCTCGGGTCACAGGCTTGGCCTTGGCCTTCCTATTCTTCGGCTT				
Lck1-12::EGFPm::CD3eBRS	For	GTACAAGCCGAAGAATAGGAAGGCCAAGGCCAAGCCTGTGACCCGAGGAACCGGTGCTGGTAGCAGGCCCAGAGGGCAAAACAAGGAGCGGTAAGC	Annealed oligos	pEGFPm-N2 Lck1-12	BsrGI/NotI	NA
	Rev	GGCCGCTTACCGCTCCTTGTTTTGCCCTCTGGGCCTGCTACCAGCACCGGTTCCTCGGGTCACAGGCTTGGCCTTGGCCTTCCTATTCTTCGGCTT				
Lck1-12::EGFPm::PHPLCδ	For	ATGGACGAGCTGTACAAGGACTCGGGCCGGGAC	PCR	pEGFPm-N2 Lck1-12	BsrGI/NotI	PH PLCδ cDNA (Gift from Georges Bismuth)
	Rev	TCTAGAGTCGCGGCCGCTTTACTGGATGTTGAGCTCC				
Lck1-12::EGFPm::Lactadherin C2	For	ATGGACGAGCTGTACAAGTCCGGACTCAGATCTTG	PCR	pEGFPm-N2 Lck1-12	BsrGI/NotI	Bovine Lactadherin cDNA
	Rev	TCTAGAGTCGCGGCCGCTCTAACAGCCCAGCAGC				
Lck1-12::EGFPm::Kras Cterm	For	GTACAAGTTCGGACTCGCTTCTAAGATGAGCAAAGATGGTAAAAAGAAGAAAAAGAAGTCAAGACAAAGTGTGTAATTATGTAAGC	Annealed oligos	pEGFPm-N2 Lck1-12	BsrGI/NotI	NA
	Rev	GGCCGCTTACATTACTACACATTTGTCTTTGACTTCTTTTTCTTCTTTTACCATCTTTGCTCATCTTAGAAGCGAGTCCGAACTT				

***Table S1*: Summary of molecular biology constructs used in this study.**

The sequence, the cloning strategy, the type of vector and the amplification matrix are summarized for each oligo corresponding to different constructs cited in this article.

Supplementary references

1. Cairo, C.W. et al. Dynamic regulation of CD45 lateral mobility by the spectrin-ankyrin cytoskeleton of T cells. *J Biol Chem* **285**, 11392-401 (2010).
2. He, H.T. & Marguet, D. Detecting nanodomains in living cell membrane by fluorescence correlation spectroscopy. *Annu Rev Phys Chem* **62**, 417-36 (2011).
3. Blouin, C.M. et al. Glycosylation-Dependent IFN-gammaR Partitioning in Lipid and Actin Nanodomains Is Critical for JAK Activation. *Cell* **166**, 920-34 (2016).